



# Hydrothermal behavior and irreversibility analysis of Bödewadt flow of radiative and dissipative ternary composite nanomaterial due to a stretched rotating disk

M.K. Sarangi<sup>a</sup>, D.N. Thatoi<sup>a</sup>, Sachin Shaw<sup>b</sup>, M. Azam<sup>c</sup>, Ali J. Chamkha<sup>d</sup>, M.K. Nayak<sup>a,e,\*</sup>

<sup>a</sup> Department of Mechanical Engineering, ITER, Siksha 'O' Anusandhan University, Bhubaneswar 751030, India

<sup>b</sup> Department of Mathematics and Statistical Sciences, Botswana International University of Science and Technology, Private Bag, 16, Palapye, Botswana

<sup>c</sup> Faculty of Engineering, Kuwait College of Science and Technology, Doha District, Kuwait

<sup>d</sup> School of Mathematics and Statistics, Yulin University, Yulin 719000, PR China

<sup>e</sup> Department of Mechanical Engineering, FET, ITER, Siksha 'O' Anusandhan Deemed to be University, Bhubaneswar 751030, India

## ARTICLE INFO

### Keywords:

Bödewadt flow  
Ternary Hybrid Nanofluid  
Second Order Slip  
Radially Stretching  
Heat Transfer  
Entropy Analysis

## ABSTRACT

Bödewadt flow and heat transfer characteristics of radiative and dissipative ternary composite nanomaterial over a stretched rotating disk is investigated. Flow is subjected to second order boundary slip. Entropy optimization due to radially stretched flow of ternary composite nanomaterial is executed. The main purpose of this novel study is to investigate the improvements in the heat transfer performance and flow behavior of the present system through the use of ternary composite nanomaterial compared to the thermal performance of hybrid and mono nanofluids subject to second order slip condition. The ternary composite/hybrid nanomaterial is a mixture of water as base fluid and  $Al_2O_3$ , Graphene and MWCNT as nanoparticles. The numerical solution is obtained by using bvp4c method through MATLAB. The most important physical conclusion of the present investigation is that introduction of ternary composite nanofluid to the Bödewadt flow over a stretched rotating disk gives rise to controlled motion subject to slip condition, reduces surface viscous drag effectively and ameliorates heat transfer rate thereby imparting significant cooling compared to binary hybrid nanofluid and mono nanofluid.

## 1. Introduction

A novel heat transfer fluid developed (first by Choi [1]) through homogenous mingling of low volume and high thermal conductivity nanoparticles in low thermal conductivity conventional fluids (enhancing their thermal performance) is popularly known as nanofluid. Several physical phenomena such as heating-cooling, friction reduction, heat transfer, drag minimization, pressure drop, energy transfer etc which when apply to nanofluids invite more interest in the research arena. For instance, Trisaksri and Wongwises [2] suggested in their research why the suspended nanoparticles can enhance the heat transfer of conventional fluids effectively. Murshed et al. [3] explored in their review analysis about the various aspects of nanofluids including synthesis, potential applications, experimental and analytical studies on the effective thermal conductivity, effective thermal diffusivity, convective heat transfer, and electro kinetic properties. Khan and Pop [4] were the pioneers who worked first on stretched surface with nanofluids. They

explored the effects of Brownian motion and thermophoresis. It was found that the reduced Nusselt number is a decreasing function of each dimensionless number, while the reduced Sherwood number is an increasing function of higher Prandtl number. Waqas [5] analyzed heat transfer in ferromagnetic stretching flow by moving surface considering a magnetic dipole. Rheological relations of non-Newtonian (Williamson) fluid are taken into account for modeling and analysis. Chemical reactions (homogeneous and heterogeneous) are considered for elaboration of mass transportation characteristics. They revealed that velocity and thermal fields have opposite behavior for ferrohydrodynamic interaction parameter. Besides the heat transportation rate is improved subjected to larger Prandtl number. Wakif et al. [6] studied the convective motion of a bi-phasic mixture near a linearly stretching sheet for a micropolar nanofluidic medium including 60 % of ethylene glycol, 40 % of pure water, and a certain volume fraction of alumina nanoparticles. They found in their investigation that the mass loading of alumina nanoparticles provides a significant thermal enhancement, speeds up its motion, and increases the coefficients of skin- friction and

\* Corresponding author at: Department of Mechanical Engineering, ITER, Siksha 'O' Anusandhan University, Bhubaneswar 751030, India.  
E-mail address: [mkn2122@gmail.com](mailto:mkn2122@gmail.com) (M.K. Nayak).

Nomenclature	
$(u, v, w)$	Velocity components in increasing $(r, \phi, z)$ directions $(m s^{-1})$
$\rho_{hnf}$	Effective density of the hybrid nanofluid $(kg m^{-3})$
$\mu_{hnf}$	Effective dynamic viscosity of the hybrid nanofluid $(kg m^{-1} s^{-1})$
$(\rho C_p)_{hnf}$	Specific heat capacity of the hybrid nanofluid $(J kg^{-2} m^3 K^{-1})$
$T$	Fluid temperature in the boundary layer $(K)$
$T_w$	Surface temperature $(K)$
$T_\infty$	Ambient fluid temperature $(K)$
$k^*$	Mean absorption coefficient
$\sigma^*$	Stefan Boltzmann constant $(Watt/m^2 K^4)$
$\Upsilon_1$	First order slip factor in radial direction
$\Upsilon_2$	Second order slip factor in radial direction
$\Upsilon_3$	First order slip factor in tangential direction
$\Upsilon_4$	Second order slip factor in tangential direction
$\rho_1$	Density of nanoparticle-1 $(Al_2O_3)$ $(kg m^{-3})$
$\rho_2$	Density of nanoparticle-2 $(CNT)$ $(kg m^{-3})$
$\rho_3$	Density of nanoparticle-3 (graphene) $(kg m^{-3})$
$\rho_{bf}$	Density of base fluid $(kg m^{-3})$
$\phi_1$	Volume fraction of nanoparticle-1 $(Al_2O_3)$
$\phi_2$	Volume fraction of nanoparticle-2 $(CNT)$
$\phi_3$	Volume fraction of nanoparticle-3 (graphene)
$\phi$	Total volume fraction of ternary hybrid nanofluid
$\mu_{nf1}$	Dynamic viscosity of nanoparticle-1 $(Al_2O_3)$ $(kg m^{-1} s^{-1})$
$\mu_{nf2}$	Dynamic viscosity of nanoparticle-2 $(CNT)$ $(kg m^{-1} s^{-1})$
$\mu_{nf3}$	Dynamic viscosity of nanoparticle-3 (graphene) $(kg m^{-1} s^{-1})$
$\mu_{bf}$	Dynamic viscosity of base fluid $(kg m^{-1} s^{-1})$
$\rho_1 C_{p1}$	Specific heat capacity of nanoparticle-1 $(Al_2O_3)$ $(J kg^{-2} m^3 K^{-1})$
$\rho_2 C_{p2}$	Specific heat capacity of nanoparticle-2 $(CNT)$ $(J kg^{-2} m^3 K^{-1})$
$\rho_3 C_{p3}$	Specific heat capacity of nanoparticle-3 (graphene) $(J kg^{-2} m^3 K^{-1})$
$C_{p,bf}$	Specific heat capacity of base fluid $(J kg^{-2} m^3 K^{-1})$
$k_{nf1}$	Thermal conductivity of nanoparticle-1 $(Al_2O_3)$ $(W m^{-1} K^{-1})$
$k_{nf2}$	Thermal conductivity of nanoparticle-2 $(CNT)$ $(W m^{-1} K^{-1})$
$k_{nf3}$	Thermal conductivity of nanoparticle-3 (graphene) $(W m^{-1} K^{-1})$
$k_{bf}$	Thermal conductivity of base fluid $(W m^{-1} K^{-1})$
$\varepsilon$	Stretching strength parameter
$L_1$	First order slip parameter in radial direction
$L_2$	Second order slip parameter in radial direction
$L_3$	First order slip parameter in tangential direction
$L_4$	Second order slip parameter in tangential direction
$p$	Pressure $(Pa)$
$Pr$	Prandtl number
$N_r$	Radiation parameter
$B_r$	Rotational Brinkman number
$Re$	Rotational Reynolds number
$E_c$	Eckert number
$\alpha$	Temperature difference parameter
bf	Base fluid
hnf	Hybrid nanofluid
p	Nano solid particles

couple-stress at the stretching sheet. Shah et al. [7] examined three-dimensional micropolar nanofluids of single and multi-walled carbon nanotubes (CNTs) dissolved in water and gasoline liquids for Bödewadt flow over a static disk. The finding reveals that with enhancement of volume fraction, the micro-rotational velocities ameliorate. Skin friction gets declined for escalating values of porosity parameter and volume fraction, while Nusselt number shows opposite behavior. Effect of multiple-walled CNTs is quite effective than that of single-walled CNTs. Farooq et al. [8] scrutinized the three-dimensional bioconvection flow performances of viscoelastic nanofluids through a elongating sheet with motile microorganisms. In their study they found that fluid temperature amplifies with higher estimations of the Brownian motion and thermophoresis parameter. The microorganism profile declines for Peclet number and bioconvection Lewis number while they upgrade for buoyancy ratio parameter and bioconvection Rayleigh number. Hayat et al. [9] examined the melting phenomenon in magnetohydrodynamic flow of Jeffrey nanomaterial by a stretching surface subject to chemical reaction. In their investigation they remarkably explored that flow can be controlled through higher estimations of the Hartman number and ratio of relaxation to the retardation time parameter. The temperature of the fluid intensifies with a larger thermophoresis parameter, Eckert number, Prandtl number, Hartman number, and velocity ratio parameter. The concentration of fluid is higher for a larger estimation of the thermophoresis parameter, Brownian motion parameter, and activation energy parameter. Further, the skin friction coefficient can be reduced via a higher melting parameter, velocity ratio parameter, and the ratio of the relaxation to the retardation time parameter. The Nusselt number is an increasing function of the Deborah number and the thermophoresis parameter. The Sherwood number is larger for a higher Brownian

motion parameter and reaction rate parameter. Pavoski et al. [10] presented a viable process for recycling a spent catalyst and synthesis of a composite likely to be applied to materials to improve or add magnetism. Nayak et al. [11] studied the MHD 3D flow and heat transfer analysis of nanofluid by shrinking surface inspired by thermal radiation and viscous dissipation. Chen et al. [12] studied Surface activated  $Co_3O_4/MoO_3$  nanostructured electrodes by air-plasma treatment toward enhanced super capacitor. Nayak et al. [13] investigated free convection and second law scrutiny of NEPCM suspension inside a wavy-baffle-equipped cylinder under altered Fourier theory. Hayat, et al. [14] analyzed melting effect in squeezing flow of third-grade fluid with non-Fourier heat flux model. Nayak et al. [15] examined electromagnetic flow of SWCNT/MWCNT suspensions with optimized entropy generation and cubic auto catalysis chemical reaction. They reveal that MWCNT is more effective in heat transfer aspects than MWCNT. Santos et al. [16] studied about the characteristics of carbon nanotubes based multi-directional strain sensor. Harish, et al. [17] discussed the amine-functionalized ZnO hierarchical nanostructures for enhanced photo catalytic decomposition under visible light illumination. Mehmood et al. [18] analyzed the effects of thermal-diffusion and diffusion-thermo on oblique stagnation point flow of couple stress Casson fluid over a stretched horizontal Riga plate with higher order chemical reaction.

Mabood et al. [19] studied EMHD flow of non-Newtonian nanofluids over thin needle with Robinson's condition and Arrhenius pre-exponential factor law. Sajjad et al. [20] investigated designing graphene oxide/silver nanoparticles based nanocomposites by energy efficient green chemistry approach and their physicochemical characterization. Alsaadi et al. [21] studied the melting effect with entropy generation minimization in flow of carbon nanotubes. They found that

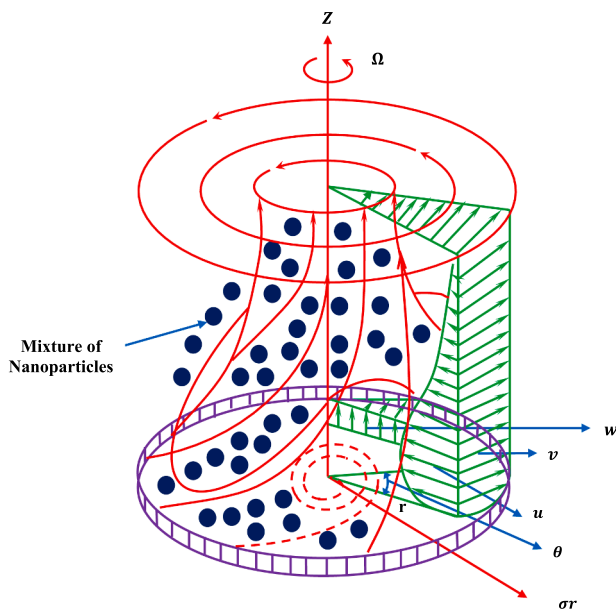


Fig. 1. Schematic representation of the Bödewadt Flow (Sahoo et al. [41]).

velocity intensifies for higher estimations of squeezing parameter, nanoparticle volume fraction and melting parameter, while it reduces the temperature of fluid.

Nevertheless, several nanofluids have been employed in diversified engineering and industrial applications in recent decades due to their better thermal properties, hybrid nanofluids were developed in order to attain more efficient results regarding heat transfer enhancement fulfilling the industrial demand of huge cooling (Babu et al. [22], Yang et al. [23]). Further, Suresh et al. [24] investigated thermal transport mechanism of  $Cu - Al_2O_3$  hybrid nanofluid. Waini et al. [25] examined the transient behavior of flow and heat transfer of hybrid nanofluid subject to stretching/ shrinking sheet. Rooman et al. [26] studied three-dimensional hybrid nanoparticles magnetohydrodynamic flow through a bidirectional exponential stretching/shrinking plate. Their study reveals that rise in magnetic parameter controls the motion of hybrid nanofluid. Nayak et al. [27] investigated the efficacy of diverse structures of wavy baffles on heat transfer amplification of double-diffusive natural convection inside a C-shaped enclosure filled with hybrid nanofluid. Muhammad et al. [28] explored the influence of squeezed flow of hybrid nanomaterial via FDM with Cattaneo-Christov (C–C) heat flux. They found in their investigation that velocity of the hybrid nanomaterial decreases with higher Hartman number and velocity slip parameter, while it increases with increase in Reynolds and squeezing parameter. Temperature of the hybrid nanomaterial increases for large Hartman number, Eckert number and squeezing parameter, Skin friction is controlled through higher Reynolds number, while it intensifies with nanoparticle volume fractions for GO and Ag. Nayak et al. [29] discussed assisting and opposing non-linear radiative flow of hybrid nanofluid past stretched cylinder. Muhammad et al. [30] studied FDM analysis for squeezed flow of hybrid nanofluid in presence of Cattaneo-Christov (CC) heat flux and convective boundary condition. Shaw et al. [31] remarkably showed hydromagnetic flow and thermal interpretations of Cross hybrid nanofluid influenced by linear, nonlinear and quadratic thermal radiations for any Prandtl number.

Ternary hybrid nanofluids (THNFs) are formed where three different types of nanoparticles are dispersed into base fluid. In general, different

sizes of nanoparticles in the nanofluid are dispersed to form an ordered arrangement of liquid molecules around the nanoparticles, thereby enhancing the thermal conductivity fulfilling the industrial demand of huge cooling.

Several experimental models of ternary composite nanofluids have been developed in the recent years in order to accomplish both improved thermophysical and heat transfer properties of ternary composite nanofluids. As a benefit, such fluids cater comfortably the vast cooling needs of present expanding industries in which mono and binary hybrid nanofluids are impeded. For instance, Ahmed et al. [32] studied heat transfer growth of sono-chemically synthesized  $ZnO + Al_2O_3 + TiO_2/DW$  based ternary hybrid nanofluids in a square flow conduit. They found that metal oxide  $ZnO + Al_2O_3 + TiO_2/DW$  based ternary hybrid nanofluids have improved thermophysical properties compared to mono and bi-hybrid nanofluids. Dezfulizadeh et al. [33] analyzed that dynamic viscosity and thermal conductivity of water-Cu-SiO<sub>2</sub>-MWCNT ternary hybrid nanofluid and formation of practical correlations. They declared their results that dynamic viscosity and thermal conductivity of water-Cu-SiO<sub>2</sub>-MWCNT ternary hybrid nanofluid enhance due to rise in volume fractions of nanoparticles. Sahoo and Kumar [34] developed a correlation to determine the viscosity of ternary hybrid nanofluid. Very recently, Sarangi et al. [35] studied influence of small and high Prandtl numbers on rotational flow and thermal behavior of ternary hybrid nanomaterials. Their numerical results conveyed that prominent decelerated flow of ternary hybrid nanofluid is attained due to amplification of rotation parameter in Darcy-Forchheimer medium subject to both low Pr ( $Pr = 0.01$ ) and high Pr ( $Pr = 10000$ ) than unary nanofluid. Axial velocity peters out by 11.76 % (at low Pr ( $Pr = 0.01$ )) and 12.5 % (at high Pr ( $Pr = 10000$ )) for ternary hybrid nanofluid (THNF) while it whittles down by 21.42 % (at low Pr) and 20 % (high Pr) for unary nanofluid (UNF) subject to fluid (UNF/THNF) flows in Darcy medium ( $Fr = 0$ ) and non-Darcy medium ( $Fr = 3$ ). In addition, heat transfer rate from the rotating surface emaciates significantly by 119 % for THNF at  $Br = 1.5$ ,  $Bi = 1$  from low Pr ( $Pr = 0.01$ ) to high Pr ( $Pr = 10000$ ).

Bödewadt flow is a kind of rotating flow which was introduced by Bödewadt [36] in 1940. This revolving flow takes place over stationary plane through the origin. At this position the fluid experiences rigid body rotation about fixed axis. In the neighborhood of the boundary the drag restrains the azimuthal velocity thereby weakens the centrifugal force. Consequently, radial pressure pushes the fluid towards the rotation axis which in turn generates the radial velocity component. To ensure the conservation of mass, the axial upward flow leads to a 3D motion. This kind of flow is experienced in many processes such as rotor-stator system and chemical mixing chambers. In view of this, modern researchers have started their investigations on Bödewadt flow several fluids subject to different geometries. For instance, Turkyilmazoglu [37] studied Bödewadt boundary layer flow of a viscous fluid using Chebyshev collocation method. Rafiq and Mustafa [38] have discussed the Bödewadt propulsion of Bingham liquids with bvp4c based collocation method. Mukherjee and Sahoo [39] have presented the Chebyshev collocation method of solutions for the Bödewadt boundary layer motion of viscous fluid in presence of Coriolis force. Do et al. [40] have analyzed response and sensitivity of Bödewadt motion to a harmonic inflection of the rotation. Sahoo et al. [41] have obtained Keller box and finite difference solutions for the Bödewadt motion of Newtonian fluid with slip effects.

As per the survey of the preceding literature, it is confirmed that numerous researches have been conducted on flow and heat transfer of single and binary composite nanofluids. However, there is no specific study carried out on flow and heat transfer of ternary composite nanofluid due to a radially stretching surface.

The objectives of the present research include:

- Analyze Bödewadt flow and heat transfer aspects of dissipative and radiative ternary composite nanofluid due to a stretched rotating disk.
- Study the impact of second order slip on rotational flow of ternary composite nanofluid.
- Investigate entropy optimization so as to scrutinize the thermal efficiency of typical system.

The novelties of the present study include:

- Introduction of ternary composite nanofluid to the Bödewadt flow over a stretched rotating disk.
- Applying ternary composite nanofluid to second order slip mechanism.
- Entropy optimization of ternary composite nanofluid subject to radially stretched flow.

## 2. Physical description of Model: Governing and similarity equations

Let us consider an incompressible flow of ternary hybrid nanofluid (THNF) over a rotating disk located at  $z = 0$  (Fig. 1). The motion arises by the rotation of the fluid like a rigid body with constant angular velocity  $\Omega$  at far distance from the disk surface. It is the steady motion of an incompressible fluid due to an infinite rotating plane lamina according to Von Karman [42]. For instance, for the rotating lamina acts as a kind of centrifugal fan, the fluid moves radially outwards, especially near the lamina, and therefore, there must be an axial motion towards the lamina in order to preserve continuity. We assume the cylindrical coordinate system  $(r, \theta, z)$  in such a manner that the disk remains stationary at  $z = 0$ . The fluid comprises of nanoparticle-1 as  $Al_2O_3$ (spherical), nanoparticle-2 as MWCNT (cylindrical), nanoparticle-3 as graphene (platelet) and base fluid as water. Due to the axial symmetry the derivatives along tangential coordinate  $\theta$  is omitted. Further assumptions made for developing modeling of the problem are:

- Flow is induced due to uniform stretching of disk in radial direction with stretching rate  $\sigma s^{-1}$ .
- THNF is steady and incompressible
- THNF is radiative and dissipative in nature
- The uniform temperature of the surface of the disk is greater than the constant temperature of revolving stream far away from the wall.
- The fluid properties such as density, viscosity, specific heat capacity and thermal conductivity vary with respect to solid volume fractions.

Using above invoked hypothesis and assumptions the governing Navier-Stokes and energy equations are (Turkyilmazoglu [37], Sibanda and Makinde [44], Muhammad et al. [45]):

Continuity Equation

$$\frac{\partial u}{\partial r} + \frac{u}{r} + \frac{\partial w}{\partial z} = 0 \tag{1}$$

Momentum equation along radial direction

$$\rho_{hnf} \left( u \frac{\partial u}{\partial r} - \frac{v^2}{r} + w \frac{\partial u}{\partial z} \right) = -\frac{\partial p}{\partial r} + \mu_{hnf} \left( \frac{\partial^2 u}{\partial r^2} + \frac{1}{r} \frac{\partial u}{\partial r} - \frac{u}{r^2} + \frac{\partial^2 u}{\partial z^2} \right) \tag{2}$$

Momentum equation along azimuthal direction

$$\rho_{hnf} \left( u \frac{\partial v}{\partial r} - \frac{uv}{r} + w \frac{\partial v}{\partial z} \right) = \mu_{hnf} \left( \frac{\partial^2 v}{\partial r^2} - \frac{v}{r^2} + \frac{1}{r} \frac{\partial v}{\partial r} + \frac{\partial^2 v}{\partial z^2} \right) \tag{3}$$

Momentum equation along axial direction

$$\rho_{hnf} \left( u \frac{\partial w}{\partial r} + w \frac{\partial w}{\partial z} \right) = -\frac{\partial p}{\partial z} + \mu_{hnf} \left( \frac{\partial^2 w}{\partial r^2} + \frac{1}{r} \frac{\partial w}{\partial r} + \frac{\partial^2 w}{\partial z^2} \right) \tag{4}$$

Energy Equation

$$\begin{aligned} (\rho C_p)_{hnf} \left( u \frac{\partial T}{\partial r} + w \frac{\partial T}{\partial z} \right) &= k_{hnf} \left( \frac{\partial^2 T}{\partial r^2} + \frac{1}{r} \frac{\partial T}{\partial r} + \frac{\partial^2 T}{\partial z^2} \right) \\ &+ \frac{16\sigma^* T_\infty^3}{3k^*} \left( \frac{\partial^2 T}{\partial r^2} + \frac{1}{r} \frac{\partial T}{\partial r} + \frac{\partial^2 T}{\partial z^2} \right) \\ &+ 2\mu_{hnf} \left[ \left( \frac{\partial u}{\partial r} \right)^2 + \frac{u^2}{r^2} + \left( \frac{\partial w}{\partial z} \right)^2 \right] \\ &+ \mu_{hnf} \left[ \left( \frac{\partial v}{\partial z} \right)^2 + \left( \frac{\partial w}{\partial r} + \frac{\partial u}{\partial z} \right)^2 + \left\{ r \frac{\partial}{\partial r} \left( \frac{v}{r} \right) \right\}^2 \right] \end{aligned} \tag{5}$$

The associated boundary conditions (Von Karman [42], Turkyilmazoglu [37], Muhammad et al. [45], Abbas et al. [46]):

$$\left. \begin{aligned} u = \sigma r + Y_1 \frac{\partial u}{\partial z} + Y_2 \frac{\partial^2 u}{\partial z^2}, v = Y_3 \frac{\partial v}{\partial z} + Y_4 \frac{\partial^2 v}{\partial z^2}, w = 0, T = T_w \text{ at } z = 0 \\ u \rightarrow 0, v \rightarrow r\Omega, T \rightarrow T_\infty \text{ as } z \rightarrow \infty \end{aligned} \right\} \tag{6}$$

The boundary conditions (6) are considered to represent the Bödewadt flow subject to second order slip and isothermal heating conditions referring to the literature (Von Karman [42], Turkyilmazoglu [37], Muhammad et al. [45], and Abbas et al. [46]). Here  $(u, v, w)$  are respectively, velocity components in increasing  $(r, \theta, z)$  directions,  $p, \rho, \mu, k, (\rho C_p)_{hnf}$  are respectively pressure, density, dynamic viscosity, thermal conductivity, specific heat capacity;  $T_w, T_\infty, k^*, \sigma^*$  are respectively boundary layer fluid temperature, wall fluid temperature, ambient fluid temperature, mean absorption coefficient, Stefan Boltzmann constant,  $Y_1, Y_2$  are first and second order slip factors in radial direction and,  $Y_3, Y_4$  are first and second order slip factors in tangential direction for velocity components  $u$  and  $v$  respectively.

It is also observed that radial pressure gradient balances the centrifugal force at the frictionless regime, that is

$$\frac{1}{\rho_{hnf}} \frac{\partial p}{\partial r} = r\Omega^2 \tag{7}$$

and in the framework of the boundary layer theory it is assumed that the viscous layer near.

the wall is also predominated by the action of the same pressure gradient.

Thermophysical properties of ternary hybrid nanofluid:

- Density

The density of ternary hybrid nanofluid (Kashyap et al. [47], Sahoo [48]):

$$\rho_{hnf} = \rho_1 \phi_1 + \rho_2 \phi_2 + \rho_3 \phi_3 + (1 - \phi_1 - \phi_2 - \phi_3) \rho_{bf}$$

where  $\rho_1, \rho_2, \rho_3$  are the densities and  $\phi_1, \phi_2, \phi_3$  are the volume fractions of nanoparticle-1, nanoparticle-2 and nanoparticle-3 respectively and  $\phi = \phi_1 + \phi_2 + \phi_3$  is the total volume fraction of ternary hybrid nanofluid. Here,  $\rho_{bf}$  is the density of base fluid.

Here, nanoparticle-1 is  $Al_2O_3$ (spherical), nanoparticle-2 is CNT (cylindrical), nanoparticle-3 is graphene (platelet) and base fluid is water.

- Viscosity

The dynamic viscosity of ternary hybrid nanofluid (Kashyap et al. [47], Sahoo [48]):

$$\mu_{hnf} = (\mu_{nf1} \phi_1 + \mu_{nf2} \phi_2 + \mu_{nf3} \phi_3) / \phi$$

Where  $\mu_{nf1} = \mu_{bf}(1 + 2.5\phi + \phi^2)$ (nanoparticle-1, spherical shape),  $\mu_{nf2} = \mu_{bf}(1 + 13.5\phi + 904.4\phi^2)$ (nanoparticle-2, cylindrical shape), and.

$\mu_{nf3} = \mu_{bf}(1 + 37.1\phi + 612.6\phi^2)$  (nanoparticle-3, platelet shape).  
 $\mu_{bf}$  is the dynamic viscosity of base fluid.

• **Specific Heat**

The specific heat capacity of ternary hybrid nanofluid (Kashyap et al. [47], Sahoo [48]):

$$(\rho C_p)_{hnf} = \rho_1 C_{p1} \phi_1 + \rho_2 C_{p2} \phi_2 + \rho_3 C_{p3} \phi_3 + (1 - \phi_1 - \phi_2 - \phi_3) \rho_{bf} C_{p,bf}$$

Where  $\rho_1 C_{p1}, \rho_2 C_{p2}, \rho_3 C_{p3}$  are specific heat capacity and  $C_{p1}, C_{p2}, C_{p3}$  are specific heats of nanoparticle-1 [ $Al_2O_3$  (spherical)], nanoparticle-2 [CNT (cylindrical)], and nanoparticle-3 [graphene (platelet)] respectively and  $C_{p,bf}$  is the specific heat of base fluid.

• **Thermal Conductivity**

The thermal conductivity of ternary hybrid nanofluid (Kashyap et al. [47], Sahoo [48]):

$$H' + 2F = 0 \tag{9}$$

$$\frac{\mu_{hnf}}{\mu_{bf}} \left[ \frac{1}{(1 - \phi_1 - \phi_2 - \phi_3) + \left(\frac{\rho_1}{\rho_{bf}}\right)\phi_1 + \left(\frac{\rho_2}{\rho_{bf}}\right)\phi_2 + \left(\frac{\rho_3}{\rho_{bf}}\right)\phi_3} \right] F'' - F'H + G^2 - F^2 - 1 = 0 \tag{10}$$

$$\frac{\mu_{hnf}}{\mu_{bf}} \left[ \frac{1}{(1 - \phi_1 - \phi_2 - \phi_3) + \left(\frac{\rho_1}{\rho_{bf}}\right)\phi_1 + \left(\frac{\rho_2}{\rho_{bf}}\right)\phi_2 + \left(\frac{\rho_3}{\rho_{bf}}\right)\phi_3} \right] G'' - 2FG - G'H = 0 \tag{11}$$

$$\left( \frac{k_{hnf}}{k_{bf}} + \frac{4}{3Nr} \right) \left[ \frac{1}{(1 - \phi_1 - \phi_2 - \phi_3) + \left(\frac{(\rho C_p)_1}{(\rho C_p)_{bf}}\right)\phi_1 + \left(\frac{(\rho C_p)_2}{(\rho C_p)_{bf}}\right)\phi_2 + \left(\frac{(\rho C_p)_3}{(\rho C_p)_{bf}}\right)\phi_3} \right] \theta'' - PrH\theta' + 2A_2 \frac{\mu_{hnf}}{\mu_{bf}} \frac{Br}{Re} [2F^2 + (H')^2] + A_2 \frac{\mu_{hnf}}{\mu_{bf}} Br [(F')^2 + 2(G')^2] = 0 \tag{12}$$

$$k_{hnf} = (k_{nf1}\phi_1 + k_{nf2}\phi_2 + k_{nf3}\phi_3) / \phi$$

$k_{nf1}, k_{nf2}, k_{nf3}$  are thermal conductivities of nanoparticle-1 [ $Al_2O_3$  (spherical)], nanoparticle-2 [CNT (cylindrical)], and nanoparticle-3 [graphene (platelet)] respectively. They are expressed in combined form as

$$\frac{k_{nfi}}{k_{bf}} = \frac{k_i + (n - 1)k_{bf} + (n - 1)\phi(k_i - k_{bf})}{k_i + (n - 1)k_{bf} - (k_i - k_{bf})}$$

Where  $i = 1, 2, 3$ . Further,  $n$  denotes the shape factor ( $n = 3/\psi$ ) and  $\psi$  is the sphericity.

For spherical shaped nanoparticle,  $\psi = 1, n = 3$

For cylindrical shaped nanoparticle,  $\psi = 0.61, n = 4.9$

For platelet shaped nanoparticle,  $\psi = 0.52, n = 5.7$

Here,  $k_{bf}$  is the thermal conductivity of base fluid.

Hence, the effective thermal conductivity for spherical, cylindrical and platelet nanoparticles are.

$$\frac{k_{nf1}}{k_{bf}} = \frac{k_1 + 2k_{bf} + 2\phi(k_1 - k_{bf})}{k_1 + 2k_{bf} - (k_1 - k_{bf})} \text{ (nanoparticle-1 of spherical shape).}$$

$$\frac{k_{nf2}}{k_{bf}} = \frac{k_2 + 3.9k_{bf} + 3.9\phi(k_1 - k_{bf})}{k_1 + 3.9k_{bf} - (k_1 - k_{bf})} \text{ (nanoparticle-2 of cylindrical shape).}$$

$$\frac{k_{nf3}}{k_{bf}} = \frac{k_2 + 4.7k_{bf} + 4.7\phi(k_1 - k_{bf})}{k_1 + 4.7k_{bf} - (k_1 - k_{bf})} \text{ (nanoparticle-3 of platelet shape).}$$

The requisite transformations:

$$\left. \begin{aligned} (u, v, w) &= \left( r\Omega F(\eta), r\Omega G(\eta), \sqrt{\Omega v_f} H(\eta) \right) \\ \theta(\eta) &= \frac{T - T_\infty}{T_w - T_\infty}, P(\eta) = \frac{p - p_\infty}{\Omega \rho_f v_f}, \eta = \sqrt{\frac{\Omega}{v_f}} z \end{aligned} \right\} \tag{8}$$

where  $\eta$  is the non-dimensional distance along the axis of rotation. Using Eq.(7), Eq.(8) and above thermophysical properties, Eqs. (1)-(6) take the form

with

$$\left. \begin{aligned} F(0) &= \varepsilon + L_1 F'(0) + L_2 F''(0), G(0) = L_3 G'(0) + L_4 G''(0), \\ H(0) &= 0, \theta(0) = 1 \text{ at } \eta = 0 \\ F(\infty) &\rightarrow 0, G(\infty) \rightarrow 1, \theta(\infty) \rightarrow 0, \text{ as } \eta \rightarrow \infty \end{aligned} \right\} \tag{13}$$

where  $\eta$  is the non-dimensional distance along the axis of rotation,  $\varepsilon = \frac{\sigma}{\Omega}$  is the stretching strength parameter,  $L_1 = \Upsilon_1 \sqrt{\frac{\Omega}{v_f}}$  and  $L_2 = \Upsilon_2 \frac{\Omega}{v_f}$  are the first and second order slip parameters in radial direction. Further,  $L_3 = \Upsilon_3 \sqrt{\frac{\Omega}{v_f}}$  and  $L_4 = \Upsilon_4 \frac{\Omega}{v_f}$  are the first and second order slip parameters in tangential direction,  $Pr = \frac{v_{bf}}{\alpha_{bf}}$  is the Prandtl number,  $Nr = \frac{k^* k_{bf}}{4\sigma^* T_\infty^3}$  is the radiation parameter,  $E_c = \frac{r^2 \Omega^2}{(C_p)_{bf} (T_w - T_\infty)}$  is the Eckert number,  $Re = \frac{r^2 \Omega}{v_{bf}}$  is the Reynolds number,  $Br = \frac{r^2 \Omega^2 \mu_{bf}}{k_{bf} \Delta T}$  is the rotational Brinkman number.

The non-dimensional local skin friction coefficient,

$$(Re_r)^{1/2} C_f = \frac{\mu_{hnf}}{\mu_{bf}} \left\{ \sqrt{[F'(0)]^2 + [G'(0)]^2} \right\} \tag{14}$$

The non-dimensional local Nusselt number,

$$(Re_r)^{-1/2} Nu_r = - \left( \frac{k_{hnf}}{k_{bf}} + \frac{4}{3Nr} \right) \theta'(0) \tag{15}$$

**3. Entropy generation analysis**

Entropy optimization is the quantity of entropy produced by irreversible processes due to thermal and fluid friction irreversibilities in the present thermodynamic system. The volumetric rate of local entropy generation of the present problem (Shah et al. [49], Shutaywi et al. [50], Rooman et al. [51], Shah et al. [52]):

**Table 1**  
Thermo-physical properties of the basefluid and nanoparticles at 300 K.

Parameters (unit)	Water	Al <sub>2</sub> O <sub>3</sub>	Graphene	MWCNT
ρ(Kg/m <sup>3</sup> )	997.1	3970	2200	2100
k(W.m/K)	0.613	40	5000	3007.4
c <sub>p</sub> (J/Kg.K)	4179	765	790	410
Shape		Spherical	Platelet	Cylinder

$$\begin{aligned}
 \dot{S}_{gen}''' &= \underbrace{\frac{k_{bf}}{T_\infty^2} \left[ \frac{k_{hnf}}{k_{bf}} + \frac{16\sigma^* T_\infty^3}{3k^3 k_{bf}} \right]}_{\text{Thermal irreversibility}} \left( \frac{\partial T}{\partial z} \right)^2 \\
 &+ \underbrace{\frac{\mu_{hnf}}{T_\infty} \left\{ 2 \left[ \left( \frac{\partial u}{\partial r} \right)^2 + \frac{1}{r^2} u^2 + \left( \frac{\partial w}{\partial z} \right)^2 \right] + \left( \frac{\partial v}{\partial z} \right)^2 + \left( \frac{\partial u}{\partial z} \right)^2 + \left[ r \frac{\partial}{\partial r} \left( \frac{v}{r} \right) \right]^2 \right\}}_{\text{Fluid friction irreversibility}} \quad (16)
 \end{aligned}$$

The right hand side of Eq. (16) comprises of two parts: the first part is the local entropy generation due to heat transfer irreversibility that contains the entropy generation by heat transfer due to axial conduction from the rotating disk and the second part is due to fluid friction irreversibility. The entropy generation number is the dimensionless form of the entropy generation rate, which represents the ratio between the actual entropy generation rate  $\dot{S}_{gen}'''$  and characteristic entropy generation rate  $\dot{S}_0'''$ .

The Von Karman transformation parameters of Eq. (8) are employed to nondimensionalize the local entropy generation given in Eq. (16). Therefore, the entropy generation number ( $N_G$ ) becomes:

$$N_G = \alpha \left( \frac{k_{hnf}}{k_{bf}} + \frac{4}{3Nr} \right) (\theta')^2 + \frac{\mu_{hnf}}{\mu_{bf}} \frac{Br}{Re} [4\{F^2 + (H')^2\} + Re\{(F')^2 + (G')^2\}] \quad (17)$$

The domination of the irreversibility mechanisms is physically significant since the entropy generation number is unable to overcome this problem. The Bejan number, which is the ratio of the entropy generation due to heat transfer to the total entropy generation, is employed to understand the entropy generation mechanisms. The Bejan number (Be) is a number that demonstrates the value of thermal irreversibility in comparison to absolute irreversibility.

$$Be = \frac{\alpha \left( \frac{k_{hnf}}{k_{bf}} + \frac{4}{3Nr} \right) (\theta')^2}{\alpha \left( \frac{k_{hnf}}{k_{bf}} + \frac{4}{3Nr} \right) (\theta')^2 + \frac{\mu_{hnf}}{\mu_{bf}} \frac{Br}{Re} [4\{F^2 + (H')^2\} + Re\{(F')^2 + (G')^2\}]} \quad (18)$$

Where  $\alpha = \frac{\Delta T}{T_\infty}$  is the non-dimensional temperature difference parameter,  $\Delta T = T_w - T_\infty$  is the temperature difference between surface and the free stream, and  $Br = \frac{\mu_{bf} \Omega^2 r^2}{k_{bf} \Delta T}$  is the rotational Brinkman number.

#### 4. Numerical procedure

The numerical approach of bvp4c MATLAB routine is implemented to solve (9)-(12), (17) and (18) with boundary conditions (19). Introducing new variables

$$y_1 = H, \quad y_2 = H', \quad y_3 = H'', \quad y_4 = G, \quad y_5 = G', \quad y_6 = \theta, \quad y_7 = \theta', \quad (19)$$

higher order derivative of each equations written with lower orders and it gives 'dydx' function in a matrix form as

$$dydx = \begin{pmatrix} y_2 \\ y_3 \\ \frac{y_1 y_3 - 0.5 y_2^2 + 2 y_4^2 - 2}{\mu_{hnf} A_1} \\ y_5 \\ \frac{-y_2 y_4 + y_1 y_5}{\mu_{bf} A_1} \\ y_7 \\ \frac{-Pr y_1 y_7 + 3 A_2 \frac{Br \mu_{hnf}}{Re \mu_{bf}} y_2^2 + 0.25 \frac{\mu_{hnf}}{\mu_{bf}} A_2 Br (y_3^2 + 8 y_5^2)}{\left( \frac{k_{hnf}}{k_{bf}} + \frac{4}{3Nr} \right) A_2} \end{pmatrix} \quad (20)$$

where  $A_1$  and  $A_2$  are defined as

$$\begin{aligned}
 A_1 &= \frac{1}{(1 - \phi_1 - \phi_2 - \phi_3) + \left( \frac{\rho_1}{\rho_{bf}} \right) \phi_1 + \left( \frac{\rho_2}{\rho_{bf}} \right) \phi_2 + \left( \frac{\rho_3}{\rho_{bf}} \right) \phi_3} \\
 A_2 &= \frac{1}{(1 - \phi_1 - \phi_2 - \phi_3) + \left( \frac{\rho C_p}{\rho C_p}_{bf} \right)_1 \phi_1 + \left( \frac{\rho C_p}{\rho C_p}_{bf} \right)_2 \phi_2 + \left( \frac{\rho C_p}{\rho C_p}_{bf} \right)_3 \phi_3}
 \end{aligned}$$

The initial 'guess' is written as

$$\text{guess} = [0, s_1, A_3, A_4, s_2, 1, s_3] \quad (21)$$

with unknowns guess  $s_1, s_2$  and  $s_3$ . Constants  $A_3$  and  $A_4$  are defined as

$$A_3 = \frac{s_2}{L_1} + \frac{L_2}{A_1 L_1} (0.5 s_1^2 + 2) - 2 \frac{L_2 L_3 A_1 s_2}{L_1 (A_1 + L_4 s_1)^2}, \quad A_4 = \frac{L_3 A_1 s_2}{A_1 + L_4 s_1}$$

Continue the process until we get a convergence and for that we bound the convergence criteria as absolute error  $|E_i|$  (tolerance =  $10^{-10}$  where errors are defined as

$$\begin{aligned}
 E_1 &= y_2(\infty, s_1) - H'(\infty), \\
 E_2 &= y_5(\infty, s_2) - G'(\infty), \\
 E_3 &= y_7(\infty, s_3) - \theta'(\infty),
 \end{aligned} \quad (22)$$

Using functions 'solinit = bvpinit (linspace (a,infinity,15),guess)' with guess in (21). We have assumed maximum value of  $\eta(\eta_\infty)$  as 15. However, the system is converged before maximum value of  $\eta$ .

#### 5. Results and discussions

This part of the investigation enshrines the physical interpretations of velocity (radial, azimuthal and axial), temperature, skin friction, Nusselt number, entropy generation number and Bejan number profiles of Bödewadt flow of Al<sub>2</sub>O<sub>3</sub>+MWCNT+Graphene+Water ternary hybrid nanofluid (THNF) over a rotating disk under the influence of significant embedded parameters. The non-dimensionalized governing equations are solved by implementing the bvp4c MATLAB routine. The ranges of the parameters chosen are  $0.1 \leq \epsilon \leq 0.4$ ,  $1 \leq Nr \leq 20$ ,  $1 \leq Re \leq 10$ ,  $0.1 \leq Br \leq 0.12$ ,  $0.1 \leq L_1 \leq 0.4$ ,  $0.1 \leq L_2 \leq 0.4$ ,  $0.1 \leq L_3 \leq 0.4$ ,  $0.1 \leq L_4 \leq 0.2$ ,  $0.1 \leq \alpha \leq 0.4$ . If the above parameters are not bounded in the respective domains, the convergence will not be properly attained. The fixed values of the parameters used in this problem are  $Nr = 20$ ,  $Pr = 7$ ,  $\epsilon = 0.4$ ,  $Br = Re = 0.1$ ,  $L_1 = L_2 = L_3 = L_4 = 0.1$ , and  $\alpha = 0.1$ . The thermophysical properties of nanoparticles and base fluid are mentioned in Table 1.

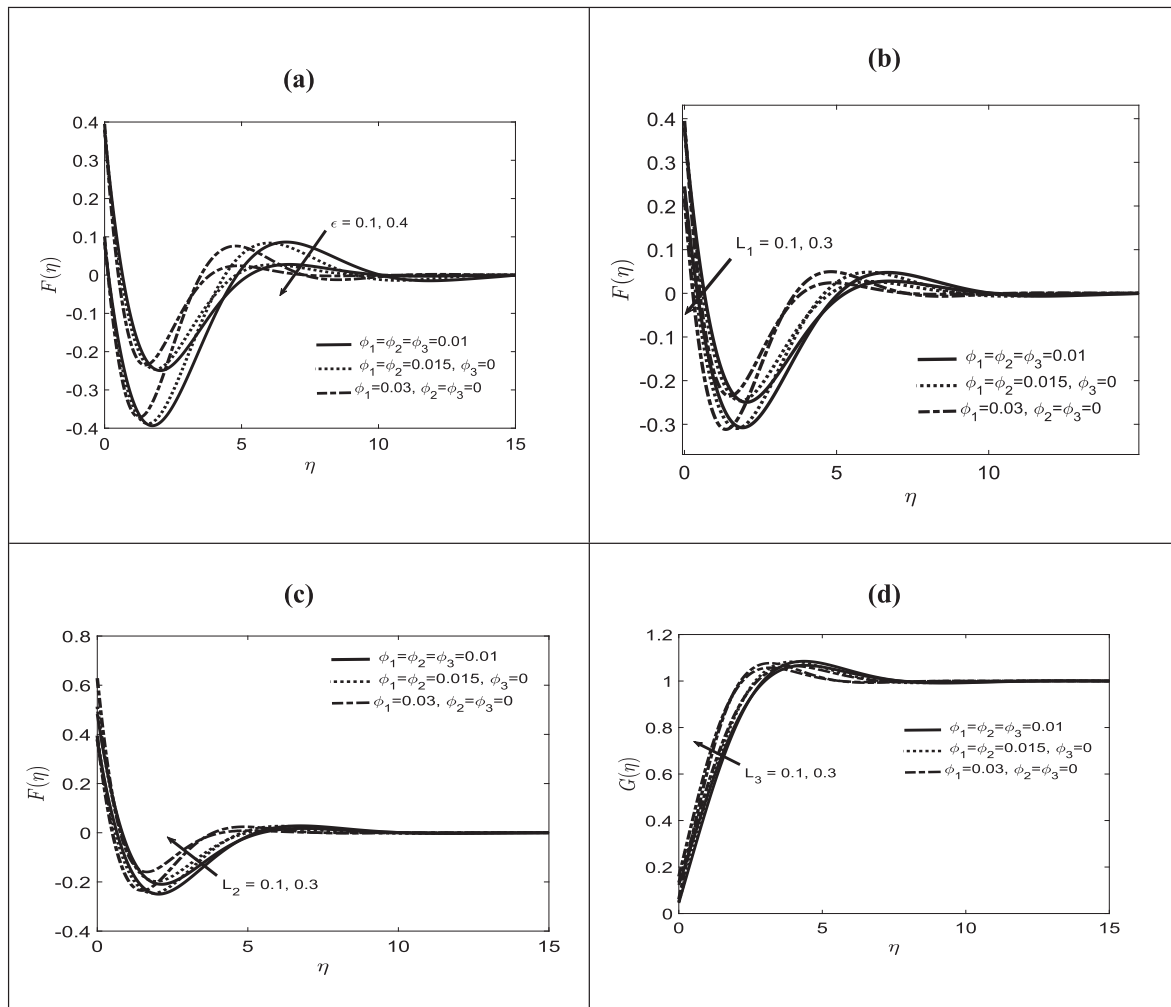


Fig. 2. (a)  $F(\eta)$  vs  $\eta$  for different  $\epsilon$  (b)  $F(\eta)$  vs  $\eta$  for different  $L_1$  (c)  $F(\eta)$  vs  $\eta$  for different  $L_2$  (d)  $G(\eta)$  vs  $\eta$  for different  $L_3$ .

5.1. Discussion of radial velocity profiles

This subsection embodies the variation of radial velocity  $F(\eta)$  for disparate  $\epsilon$ ,  $L_1$  and  $L_2$  for mono nanofluid (represented by dash line), binary hybrid nanofluid (represented by dot line) and ternary hybrid nanofluid (represented by solid line). It seems from the Fig. 2(a) that radial velocity  $F(\eta)$  enhances with rise in stretching strength parameter  $\epsilon$  ( $\epsilon = 0.1, 0.4$ ) for mono nanofluid ( $\phi_1 = 0.03, \phi_2 = \phi_3 = 0$ ), binary hybrid nanofluid ( $\phi_1 = \phi_2 = 0.015, \phi_3 = 0$ ) and ternary hybrid nanofluid ( $\phi_1 = \phi_2 = \phi_3 = 0.01$ ) effectively. However, amplification of  $\epsilon$  ( $\epsilon = 0.1, 0.4$ ) gives rise to the diminution of  $F(\eta)$  for mono nanofluid ( $\phi_1 = 0.03, \phi_2 = \phi_3 = 0$ ), binary hybrid nanofluid ( $\phi_1 = \phi_2 = 0.015, \phi_3 = 0$ ) and ternary hybrid nanofluid ( $\phi_1 = \phi_2 = \phi_3 = 0.01$ ) prominently after the cross overs away from the surface of the disk. The radial velocity profile reveals that direction of the flow is radially inward in the vicinity of the disk and at a certain distance from the disk it appears to be radially outward. Due to this fact the radial velocity attains negative values near the wall and positive values away from the wall. At fixed  $\epsilon$  (for example,  $\epsilon = 0.1$ ),  $F(\eta)$  of THNF (represented by solid line) decreases in the vicinity of the solid boundary, then attains minimum value in  $0 < \eta < 5$ . After that it follows up trend and attains maximum value in  $5 < \eta < 10$  and then with no variation towards the distance  $\eta$ . Further,  $F(\eta)$  of binary hybrid nanofluid (indicated by dotted line) follows the same trend but attaining the minimum and maximum values a little earlier distance than the previous case. In addition,  $F(\eta)$  of mono nanofluid (highlighted by dash line) follows the same nature, however, attains its minimum and maximum values well before previous cases

(both minimum and maximum values were attained in  $(5 < \eta < 10)$ ). Again, at fixed  $\epsilon$  ( $\epsilon = 0.4$ ) all three types of fluids follow the same trend but attaining lower magnitude of maxima and minima than that of  $\epsilon = 0.1$ . The  $F(\eta)$  variations of all three types of fluids disappear towards the ambient fluid that is radial velocity profiles exhibit asymptotic behavior towards the ambient fluid. Fig. 2(b) delineates the  $F(\eta)$  variations for diverse  $L_1$  for mono nanofluid ( $\phi_1 = 0.03, \phi_2 = \phi_3 = 0$ ), binary hybrid nanofluid ( $\phi_1 = \phi_2 = 0.015, \phi_3 = 0$ ) and ternary hybrid nanofluid ( $\phi_1 = \phi_2 = \phi_3 = 0.01$ ). In this case,  $F(\eta)$  decreases for rise in  $L_1$  ( $L_1 = 0.1, 0.3$ ) for all three types of fluids within few layers of the boundary layer ( $0 < \eta < 5$ ), however, the trend reverses for all beyond  $\eta = 5$ . As slip parameter rises, this allows more fluid to slip past the disk, the maximum radial velocity decreases and its location also moves towards the wall. This is because of the decreasing trend of centrifugal force. Such nature of flow appears in real world applications like polymeric solutions, suspensions, emulsions, foams (where fluid behaves as a particulate) and electrochemical industry. At fixed  $L_1$  ( $L_1 = 0.1$ , say),  $F(\eta)$  whittles down drastically and attains its lowest magnitude and then follows uptrend till it avails its highest magnitude following by diminishing trend towards the ambient irrespective of the nature of the fluid (mono nanofluid - represented by dash line, binary hybrid nanofluid - represented by dot line and ternary hybrid nanofluid - represented by solid line). Further, in the presence of slip environment, ternary hybrid nanofluid attains least value of radial velocity compared to mono nanofluid and hybrid nanofluid. In fact, inclusion of more and more nanoparticles leads to the amelioration of fluid viscosity thereby emaciating fluid velocity effectively. The

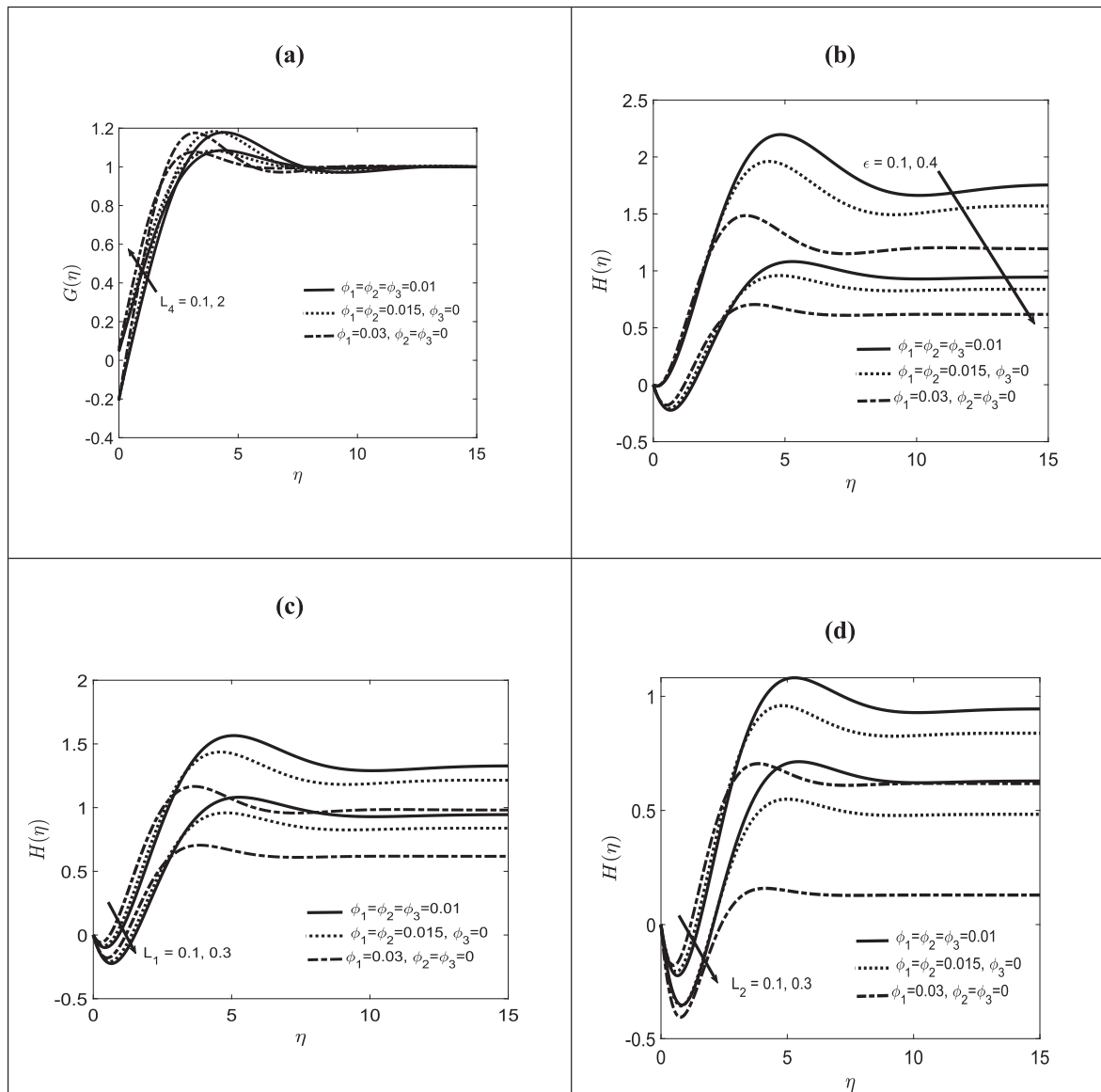


Fig. 3. (a)  $G(\eta)$  vs  $\eta$  for different  $L_4$  (b)  $H(\eta)$  vs  $\eta$  for different  $\epsilon$  (c)  $H(\eta)$  vs  $\eta$  for different  $L_1$  (d)  $H(\eta)$  vs  $\eta$  for different  $L_2$ .

variations of  $F(\eta)$  for disparate  $L_2$  subject to three types of fluids chosen in the present investigation are manifested in Fig. 2(c). This figure reveals that raise in  $L_2$  ( $L_2 = 0.1, 0.3$ ) yields the diminution of  $F(\eta)$  for all three types of fluids (mono, binary hybrid and ternary hybrid nanofluids). More evidently,  $F(\eta)|_{\text{Ternary hybrid nanofluid}} < F(\eta)|_{\text{Binary hybrid nanofluid}} < F(\eta)|_{\text{Mono nanofluid}}$  for fixed  $\epsilon = 0.1$ . At each fixed  $L_2$ ,  $F(\eta)$  diminishes effectively in the regime nearer to the solid boundary for each type of fluid. Each fluid then attains its lowest magnitude (THNF attains the lowest among three types of fluids) within few distances from the disk wall. Near  $\eta = 5$ , fluid velocity for each type of fluid up lifts and finally shows no variation towards the ambient fluid (showing asymptotic behavior). Above all, the radial component of velocity, near the disk remains negative for all values of the slip parameters ( $L_1$  &  $L_2$ ), reverses the direction away from the disk, and finally approaches its asymptotic value. Therefore, cross-overs appear in the radial velocity profile.

### 5.2. Discussion of azimuthal velocity profiles

This subsection is enshrouded with the information regarding the characteristics of azimuthal velocity profiles for varied estimations of

$L_3, L_4$  for mono nanofluid ( $\phi_1 = 0.03, \phi_2 = \phi_3 = 0$ ), binary hybrid nanofluid ( $\phi_1 = \phi_2 = 0.015, \phi_3 = 0$ ) and ternary hybrid nanofluid ( $\phi_1 = \phi_2 = \phi_3 = 0.01$ ). Fig. 2(d) explains that enlarging  $L_3$  ( $L_3 = 0.1, 0.3$ ) upsurges the azimuthal velocity  $G(\eta)$  of three types of fluids contiguous to the surface of the disk and shows reverse behavior away from the surface thereby producing cross overs in the boundary layer and finally adopting asymptotic nature towards the distant fluid (Sahoo et al. [41]). The variation of  $G(\eta)$  is marginal for all types of fluids. At fixed  $L_3$  ( $L_3 = 0.1, say$ ),  $G(\eta)$  has highest magnitude for mono nanofluid (indicated by dashed line) among binary hybrid nanofluid (indicated by dotted line) and THNF (indicated by solid line). Evidently,  $G(\eta)|_{\text{Ternary hybrid nanofluid}} < G(\eta)|_{\text{Binary hybrid nanofluid}} < G(\eta)|_{\text{Mono nanofluid}}$  for fixed  $L_3 = 0.1$ . Fig. 3(a) demonstrates  $G(\eta)$  variation for different  $L_4$  for all three types of fluids. The variations are effective. Amplifying  $L_4$  ( $L_4 = 0.1, 2$ ) yields the augmentation of  $G(\eta)$  for mono nanofluid ( $\phi_1 = 0.03, \phi_2 = \phi_3 = 0$ ), binary hybrid nanofluid ( $\phi_1 = \phi_2 = 0.015, \phi_3 = 0$ ) and ternary hybrid nanofluid ( $\phi_1 = \phi_2 = \phi_3 = 0.01$ ) near the wall. The variation is prominent near the disk for each type of fluid. The azimuthal velocity profiles reverse the direction away from the disk and approach the asymptotic value at a shorter distance from the disk as compared to the former case. However, at each  $L_4$  ( $L_4 = 0.1$ ),  $G(\eta)$  has

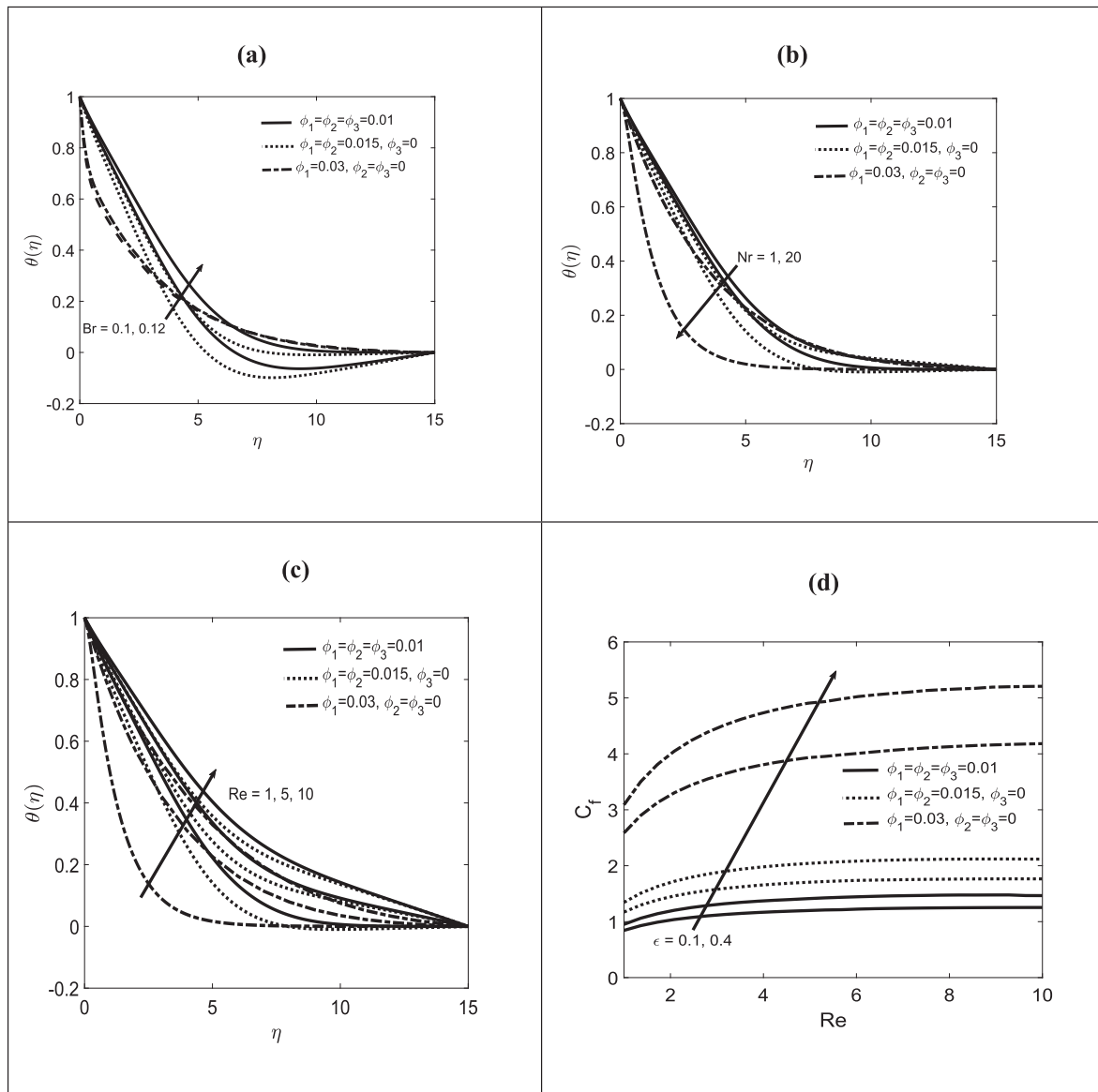


Fig. 4. (a)  $\theta(\eta)$  vs  $\eta$  for different  $Br$  (b)  $\theta(\eta)$  vs  $\eta$  for different  $Nr$  (c)  $\theta(\eta)$  vs  $\eta$  for different  $Re$  (d)  $C_f$  vs  $Re$  for different  $\epsilon$ .

**Table 2**  
Skin friction for different parameters with comparison of general, hybrid and ternary nanofluid.

$\epsilon$	$L_1$	$L_2$	$L_3$	$L_4$	$(Re_r)^{1/2} C_f$		
					$\phi_1 = \phi_2 = \phi_3 = 0.01$	$\phi_1 = \phi_2 = 0.015, \phi_3 = 0$	$\phi_1 = 0.03, \phi_2 = \phi_3 = 0$
0.4	0.1	0.1	0.1	0.1	0.95162136	1.34556516	3.08847518
0.2					1.24276779	1.77058460	4.12516760
0.4	0.2				1.43584114	2.06816101	4.94565941
	0.3				1.34545684	1.91937112	4.46506335
		0.2			1.28449434	1.82188828	4.17500346
		0.3			1.52041322	2.22845765	5.69358191
			0.2		1.63042203	2.44973247	6.99770556
			0.3		1.40940592	2.03174509	4.86597796
				1	1.38301166	1.99467996	4.78017783
				2	1.08502571	1.99915927	4.74895785
					1.22512742	2.15600574	4.99413079

highest magnitude for mono nanofluid and least magnitude for THNF and intermediate magnitude for binary hybrid nanofluid. Irrespective the nature of fluid (mono nanofluid/ binary hybrid nanofluid/ THNF),

$G(\eta)$  enhances sharply with rise in  $\eta$  (as we proceed away from the disk wall) and attains a peak value following by descending trend for few distance within the boundary layer and then all profiles merge at large

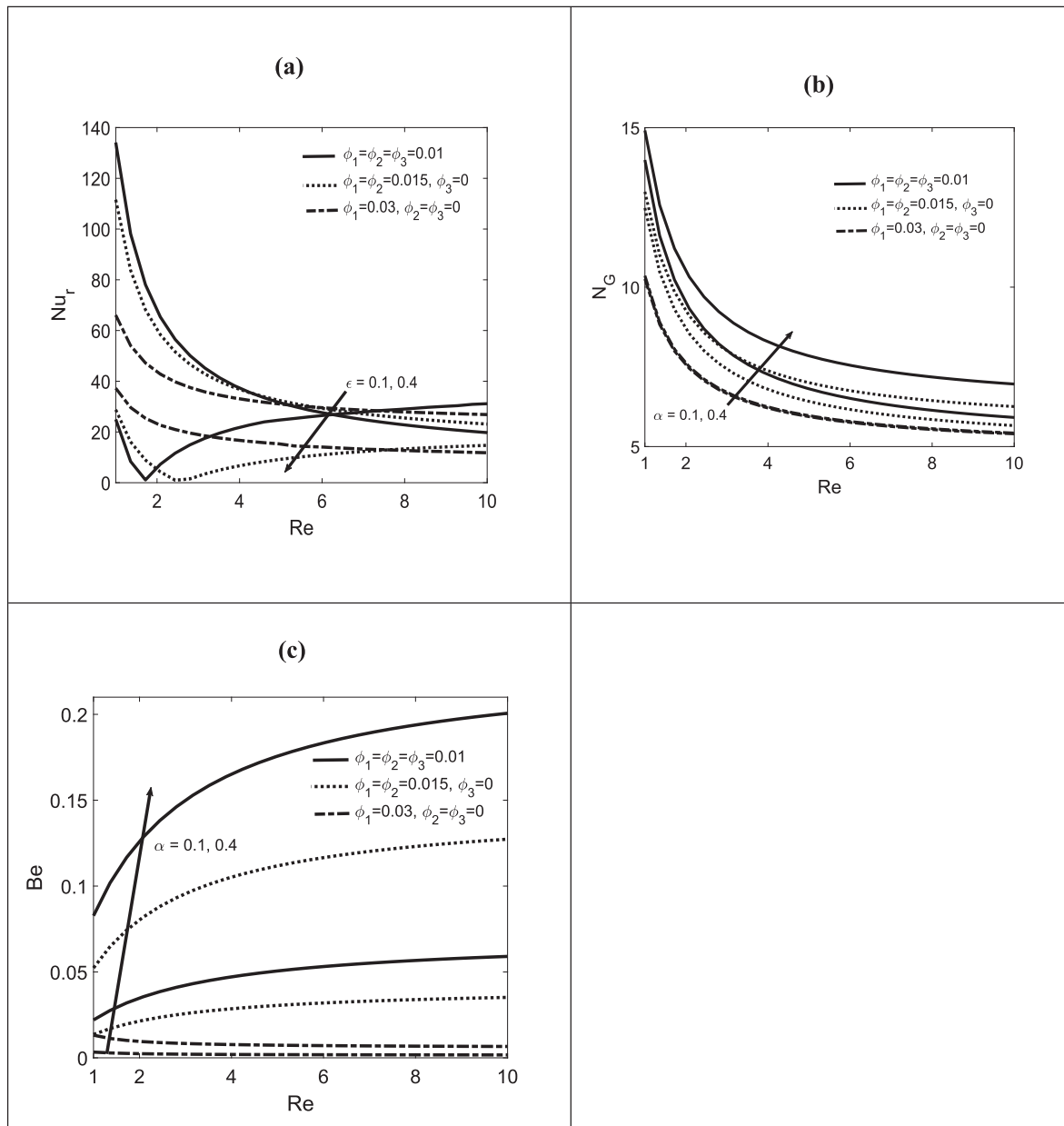


Fig. 5. (a)  $Nu_r$  vs  $Re$  for different  $\epsilon$  (b)  $N_G$  vs  $Re$  for different  $\alpha$  (c)  $Be$  vs  $Re$  for different  $\alpha$ .

**Table 3**  
Nusselt number for different parameters with comparison of general, hybrid and ternary nanofluid.

$Br$	$Nr$	$Re$	$(Re_r)^{-1/2} Nu_r$		
			$\phi_1 = \phi_2 = \phi_3 = 0.01$	$\phi_1 = \phi_2 = 0.015, \phi_3 = 0$	$\phi_1 = 0.03, \phi_2 = \phi_3 = 0$
0.1	20	0.1	50.63077060	29.15382342	1.03425346
			55.04737407	32.69590578	1.63222514
0.11	10	0.12	54.64591416	32.39083741	1.46055694
			55.45327869	33.00541811	1.28779821
0.12	15	1	55.45031554	33.00245547	1.28561506
			58.86057932	35.56265422	0.10021757
		5	59.16384557	35.79035911	0.22369368

distance from the wall.

### 5.3. Discussion of axial velocity profiles

This subsection covers the axial velocity variation for disparate  $\epsilon, L_1, L_2$  for mono nanofluid ( $\phi_1 = 0.03, \phi_2 = \phi_3 = 0$ ), binary hybrid nanofluid ( $\phi_1 = \phi_2 = 0.015, \phi_3 = 0$ ) and ternary hybrid nanofluid ( $\phi_1 = \phi_2 = \phi_3 = 0.01$ ). Fig. 3(b) acknowledges that  $H(\eta)$  of THNF (indicated by solid lines), binary hybrid nanofluid (indicated by dotted lines) and mono nanofluid (indicated by dashed lines) peter out very effectively with amplification of  $\epsilon$  ( $\epsilon = 0.1, 0.4$ ) throughout the flow domain except the region contiguous to the solid wall (Sahoo et al. [41]). This is because for larger values of  $\epsilon$  away from the disk the rotational effect dominates over the stretching effect and therefore

**Table 4**  
Entropy generation for different parameters with comparison of general, hybrid and ternary nanofluid.

Br	Nr	Re	$\alpha$	$N_G$		
				$\phi_1 = \phi_2 = \phi_3 = 0.01$	$\phi_1 = \phi_2 = 0.015,$ $\phi_3 = 0$	$\phi_1 = 0.03,$ $\phi_2 = \phi_3 = 0$
0.1	20	0.1	0.1	9.40001365	7.79319131	5.28501100
0.11				10.76037681	9.08064182	6.45045839
0.12				11.70407106	9.88567504	7.03828151
	10			9.81674673	8.27565088	5.86282834
				15	9.81672718	8.27567028
		1		1.74240239	1.45245641	1.02220701
		5		1.02480723	0.84606223	0.59271043
			0.2	10.14891182	8.46620629	5.86987223
			0.4	10.81330065	8.84733649	5.88385018

**Table 5**  
Bejan number for different parameters with comparison of general, hybrid and ternary nanofluid.

Br	Nr	Re	$\alpha$	Be		
				$\phi_1 = \phi_2 = \phi_3 = 0.01$	$\phi_1 = \phi_2 = 0.015,$ $\phi_3 = 0$	$\phi_1 = 0.03,$ $\phi_2 = \phi_3 = 0$
0.1	20	0.1	0.1	0.02946511	0.01908383	0.00977969
0.11				0.03042659	0.02059966	0.00139133
0.12				0.02756677	0.01857068	0.00159249
	10			0.03384255	0.02303067	0.00118272
				15	0.03384063	0.02302838
		1		0.21483651	0.15236144	0.00004134
		5		0.36904396	0.26492299	0.00035518
			0.2	0.06546405	0.04501783	0.00238131
			0.4	0.12288363	0.08615705	0.00475130

maxima occur there. It is here to be noted that  $H(\eta)|_{\text{Mono nanofluid}} > H(\eta)|_{\text{Binary hybrid nanofluid}} > H(\eta)|_{\text{Ternary hybrid nanofluid}}$  for fixed  $\varepsilon = 0.1$  in the flow region adjacent to the wall. At fixed  $\varepsilon (\varepsilon = 0.1, \text{ say})$ ,  $H(\eta)$  for THNF accelerates just after few layers of fluid from the wall following its attainment of peak value at  $\eta = 5$ . After that it decays prominently as we move away from the wall. The other two types of fluids namely binary hybrid nanofluid and mono nanofluid exhibit the same trend with attainment of peaks little earlier than THNF. Fig. 3(c) manifests that rise in  $L_1 (L_1 = 0.1, 0.3)$  diminishes  $H(\eta)$  for all three types of fluids (mono nanofluid, binary/ternary hybrid nanofluids) very prominently within few distances from the solid wall ( $\eta < 5$ ). At fixed  $L_1 (L_1 = 0.3, \text{ say})$ ,  $H(\eta)$  of THNF has lowest magnitude (indicated by solid line within  $\eta < 5$ ) following by binary hybrid nanofluid (indicated by dotted line within  $\eta < 5$ ) in turn following by mono nanofluid (indicated by dash line within  $\eta < 5$ ). Fig. 3(d) reveals that  $H(\eta)$  whittles down due to rise in  $L_2 (L_2 = 0.1, 0.3)$  for THNF, binary hybrid nanofluid, and mono nanofluid (represented by dashed lines) in the far side of the boundary layer region. However, at fixed  $L_2$ , each type of fluid (irrespective of their nature) rises very sharply from their least values near the wall and there after attains their peak values following declining trend towards the ambient.

**Table 6**  
Comparison of the present numerical results for  $F'(0)$  and  $G'(0)$  with Turkiymazoglu [37] and Mustafa et al. [43] with  $Pr = 1, L_1 = L_2 = L_3 = L_4 = Br = 0, N_r \rightarrow \infty$  and  $\phi = 0$ .

$\varepsilon$	$F'(0)$			$G'(0)$		
	Turkiymazoglu [37]	Mustafa et al. [43]	Present	Turkiymazoglu [37]	Mustafa et al. [43]	Present
1	-1.865469	-1.865469	-1.86546904	0.685170	0.685170	0.68517021
5	-13.46623	-13.46623	-13.4662312	1.200076	1.200076	1.20007620
10	-37.36036	-37.36036	-37.3603642	1.678166	1.678167	1.67816694
20	-105.1535	-105.1535	-105.153533	2.366480	2.366484	2.36648372

5.4. Discussion of temperature profiles

This subsection reveals the thermal field characteristics under the influences of several parameters such as  $Br, Nr, Re$  for mono nanofluid ( $\phi_1 = 0.03, \phi_2 = \phi_3 = 0$ ), binary hybrid nanofluid ( $\phi_1 = \phi_2 = 0.015, \phi_3 = 0$ ) and ternary hybrid nanofluid ( $\phi_1 = \phi_2 = \phi_3 = 0.01$ ). Fig. 4(a) implicates that rise in  $Br$  uplifts  $\theta(\eta)$  profiles for all three types of fluids in the entirety of the flow domain. Rotational Brinkman number is the ratio of direct heat conduction from the disk surface to the viscous heat generated by shear in the boundary layer. More Brinkman number implies more heat conducted into the fluid from the wall compared to heat generated due to fluid friction in the boundary layer. At fixed  $Br (Br = 0.1, \text{ say})$ ,  $\theta(\eta)$  attains its highest value for THNF (marked by solid line) following by intermediate value for binary hybrid nanofluid (marked by dotted line) and least value for mono nanofluid (marked by dash line). Mono nanofluid ( $\phi_1 = 0.03, \phi_2 = \phi_3 = 0$ ) has thinnest thermal boundary layer compared to other two types of fluids. Fig. 4(b) reveals that hike in radiation parameter  $Nr (Nr = 1, 20)$  belittles  $\theta(\eta)$  distributions for all three types of fluids. In fact, radiation parameter  $Nr$  is inversely proportional to the mean absorption coefficient. Therefore, rise in radiation parameter reduces mean absorption coefficient thereby decreasing fluid temperature. At fixed  $Nr (Nr = 20, \text{ say})$ ,  $\theta(\eta)$  is most intensified for THNF (highlighted by solid line) while it is moderately intensified for binary hybrid nanofluid (highlighted by dotted line) and least intensified for mono nanofluid (highlighted by dashed line). Thermal boundary layer thickness is least for mono nanofluid compared to that of other two types of nanofluids. Fig. 4(c) reveals the variation of  $\theta(\eta)$  in response to diverse Reynolds number  $Re$  for three different types of fluids. It is visualized that  $\theta(\eta)$

**Table 7**  
Comparison of the present numerical results for  $-\theta'(0)$  with Turkiymazoglu [37] and Mustafa et al. [43] with  $Pr = 1, L_1 = L_2 = L_3 = L_4 = Br = 0, N_r \rightarrow \infty$  and  $\phi = 0$ .

$\varepsilon$	Turkiymazoglu [38]	Mustafa et al. [39]	Present
1	0.5471813	0.5430800	0.54702913
5	1.8835820	1.8835818	1.88358292
10	2.6866575	2.6866568	2.68665679
20	3.8075476	3.8075457	3.80754721

profiles intensify due to amplification of  $Re$  ( $Re = 1, 5, 10$ ) for three types of fluids. Reynolds number is the ratio of fluid momentum force to viscous force. Therefore, rise in Reynolds number leads to greater fluid momentum force compared to viscous force. As a result, intermolecular collisions increase. Consequently, kinetic energies of the particles ameliorate thereby upsurges the fluid temperature. At particular  $Re$  ( $Re = 1$ , say) fluid temperature and the corresponding boundary layer thickness grows effectively for mono nanofluid (shown by dashed line), binary hybrid nanofluid (shown by dotted line) and ternary hybrid nanofluid (shown by solid line). It is also visualized that  $\theta(\eta)$  has least magnitude for mono nanofluid compared to other two fluids.

### 5.5. Discussion of skin friction (surface viscous drag) and Nusselt number (heat transfer rate) profiles

This subsection conveys the skin friction ( $C_f$ ) and Nusselt number variations for disparate  $\varepsilon$  against  $Re$  for mono nanofluid ( $\phi_1 = 0.03, \phi_2 = \phi_3 = 0$ ), binary hybrid nanofluid ( $\phi_1 = \phi_2 = 0.015, \phi_3 = 0$ ) and ternary hybrid nanofluid ( $\phi_1 = \phi_2 = \phi_3 = 0.01$ ). Skin friction or surface viscous drag enhances with growth in  $\varepsilon$  ( $\varepsilon = 0.1, 0.4$ ) for all three types of fluids at every value of  $Re$  ( $0 \leq Re \leq 10$ ). For greater  $\varepsilon$ , stretching effect dominates over rotational effect at fixed Reynolds number thereby intensifies surface viscous drag. At fixed  $\varepsilon$  ( $\varepsilon = 0.1$ ),  $C_f$  rises for THNF (displayed by solid line), binary hybrid nanofluid (displayed by dotted line) and mono nanofluid (displayed by dashed line) effectively (see Fig. 4(d)). In fact,  $C_f$  enhancement is very prominent for mono nanofluid compared to others. Further, highest skin friction is offered by mono nanofluid than binary hybrid nanofluid and THNF for any  $Re$  ( $0 \leq Re \leq 10$ ). Furthermore, for fixed  $\varepsilon$  ( $\varepsilon = 0.1$ ) and for specific fluid (THNF, say),  $C_f$  ameliorates as  $Re$  grows and it becomes stagnant for higher  $Re$  (towards  $Re = 10$ ). Striking Table 2, it is revealed the nature of surface viscous drag subject to THNF, binary hybrid nanofluid and mono nanofluid under the influence of varied  $\varepsilon, L_1, L_2, L_3, L_4$ . It is understood that surface viscous drag intensifies for all three types of fluids (THNF, binary hybrid nanofluid and mono nanofluid) with rise in  $\varepsilon, L_2, L_4$  while it fades away with that of  $L_1$  &  $L_3$ . Fig. 5(a) illustrates that increment in  $\varepsilon$  ( $\varepsilon = 0.1, 0.4$ ) reduces the Nusselt number ( $Nu_r$ ) against  $Re$  for three types of fluids. For greater  $\varepsilon$ , stretching effect dominates over rotational effect at fixed Reynolds number thereby reduces the fluid velocity. Therefore, particles spend more time in the vicinity of the wall and raises fluid temperature. As a result, Nusselt number (heat transfer rate) peters out. At fixed  $\varepsilon$  ( $\varepsilon = 0.1$ ), heat transfer rate attains highest for THNF (sketched by solid line), intermediate value for binary hybrid nanofluid (sketched by dotted line) and least value for mono nanofluid (sketched by dash line) within  $Re < 6.5$  (approximately). Further, at fixed  $\varepsilon$ ,  $Nu_r$  peters out with gradual growth of  $Re$  effectively. It is concluded that the heat transfer rate is prominent for THNF than others as expected. Table 3 ensures the Nusselt number behavior of mono nanofluid, binary hybrid nanofluid and THNF in response to disparate  $Br, Nr$  &  $Re$ . It is apparent that  $Re^{-\frac{1}{2}} Nu_r$  (heat transfer rate) uplifts for mono nanofluid, binary hybrid nanofluid and THNF with rise in  $Re$ . However, the enhancement is more significant for THNF compared to binary hybrid nanofluid and mono nanofluid. However, heat transfer from solid wall whittles down subject to all three fluids under the impact of  $Nr$  &  $Br$ .

### 5.6. Discussion of entropy generation and Bejan number profiles

This subsection briefs about entropy generation number and Bejan number profiles analysis for mono nanofluid ( $\phi_1 = 0.03, \phi_2 = \phi_3 = 0$ ), binary hybrid nanofluid ( $\phi_1 = \phi_2 = 0.015, \phi_3 = 0$ ) and ternary hybrid nanofluid ( $\phi_1 = \phi_2 = \phi_3 = 0.01$ ) under the influence of no-dimensional temperature difference parameter  $\alpha$  against Reynolds number  $Re$ . Entropy generation number ( $N_G$ ) ameliorates with amplification of temperature difference parameter  $\alpha$  ( $\alpha = 0.1, 0.4$ ) for three types of fluids against  $Re$  (See Fig. 5 (b)). Entropy minimization could be accomplished

with amplification of temperature difference parameter thereby leading to (less energy loss) enhancement of thermal efficiency of typical physical system. At specific  $\alpha$  ( $\alpha = 0.1$ , say),  $N_G$  attains the highest value (indicated solid line), intermediate value (indicated by dotted line) and least value (indicated by dashed line) at all  $Re$  ( $0 \leq Re \leq 10$ ). Further, at particular  $\alpha, N_G$  emaciates with gradual increment in  $Re$ . In addition, Table 4 informs about the entropy generation behavior for all three fluids subject to varied  $Br, Nr, Re, \alpha$ . The entropy generation ameliorates due to rise in  $Br, Nr, \alpha$  while it decays down for hike in  $Re$ . Fig. 5(c) identifies Bejan number ( $Be$ ) variation under the impact of  $\alpha$  against  $Re$  for three types of fluids chosen. It is envisioned that  $Be$  up lifts with rise in  $\alpha$  ( $\alpha = 0.1, 0.4$ ) for three types of fluids against  $Re$ . Here,  $Be$  attains highest value for THNF (exhibited by solid lines corresponding to  $\alpha = 0.1$  &  $\alpha = 0.4$  respectively), intermediate value (exhibited by dotted lines corresponding to  $\alpha = 0.1$  &  $\alpha = 0.4$  respectively) and least value (exhibited by dash lines corresponding to  $\alpha = 0.1$  &  $\alpha = 0.4$  respectively) for all chosen  $Re$ . It is remarkable to note here that  $Be$  enhances with gradual augmentation of  $Re$  irrespective of value of  $\alpha$  and the type of fluids considered. In addition, Table 5 provides the Bejan number ( $Be$ ) characteristics subject to flow of THNF, binary hybrid nanofluid and mono nanofluid under the influence of varied  $Br, Nr, Re, \alpha$ . As observed,  $Be$  enhances due to increment in  $Nr, Re, \alpha$  while it shows adverse effect with that of  $Br$ .

### 5.7. Validation

The results of present numerical scheme have been compared with the works of Turkyilmazoglu [37] and Mustafa et al. [43] for  $F'(0), G'(0)$  and  $\theta'(0)$ , and the results are displayed in tables 6 and 7. We have found a very good agreement with their works and it gives us confidence about the present numerical results.

## 6. Conclusion

In the present study, Bödewadt flow of radiative and dissipative ternary composite nanomaterial over a rotating disk has been investigated. The problem was modeled by considering water as base fluid and  $Al_2O_3$ , Graphene and MWCNT as nanoparticles. The simulation process was devised by adopting bvp4c method through MATLAB. The outcomes of the investigation are that rise in stretching strength parameter yields effective radial as well as axial decelerated flow for mono, binary and ternary hybrid nanofluids. Radial velocity  $F(\eta)$  exhibits opposite effect in response to amplified  $L_1$  &  $L_2$ . Azimuthal velocity  $G(\eta)$  is an increasing function of  $L_3$  &  $L_4$ . Hiked radiation parameter and rotational Brinkman number elevated fluid temperature  $\theta(\eta)$  while that of Reynolds number exhibits reverse trend in case of all three types of fluids. Surface viscous drag intensifies with rise in Reynolds number. The enhancement of heat transfer rate is more significant for ternary composite nanofluid compared to binary hybrid nanofluid and mono nanofluid. Entropy minimization could be accomplished by keeping temperature difference parameter as minimum thereby leading to (less energy loss) enhancement of thermal efficiency of typical physical system.

### Declaration of Competing Interest

The authors declare that they have no known competing financial interests or personal relationships that could have appeared to influence the work reported in this paper.

### Data availability

No data was used for the research described in the article.

## Acknowledgements

This research did not receive any specific grant from funding agencies in the public, commercial, or not-for-profit sectors.

## References

- [1] S.U. Choi, J.A. Eastman, Enhancing Thermal Conductivity of Fluids with Nanoparticles, Argonne National Lab, IL (United States), 1995.
- [2] V. Trisaksri, S.J.R. Wongwises, Critical review of heat transfer characteristics of nanofluids, *Renew. Sust. Energ. Rev.* 11 (3) (2007) 512–523.
- [3] S. Murshed, K. Leong, C.J. Yang, Thermophysical and electrokinetic properties of nanofluids—a critical review, *Appl. Therm. Eng.* 28 (17–18) (2008) 2109–2125.
- [4] W.A. Khan, I. Pop, Boundary layer flow of a nanofluid past a stretching sheet, *Int. J. Heat Mass Transf.* 53 (2010) 2477–2483.
- [5] M. Waqas, A mathematical and computational framework for heat transfer analysis of ferromagnetic non-Newtonian liquid subjected to heterogeneous and homogeneous reactions, *J. Magn. Magn. Mat.* 493 (2020), 165646.
- [6] A. Wakif, M. Zaydan, A.S. Alshomrani, T. Muhammad, R. Sehaqui, New insights into the dynamics of alumina-(60% ethylene glycol + 40% water) over an isothermal stretching sheet using a renovated Buongiorno's approach: A numerical GDQLM analysis, *Int. Commun. Heat Mass Transfer* 133 (2022), 105937.
- [7] Z. Shah, M. Rooman, M. AsifJan, N. Vrinceanu, W. Deebani, M. Shutaywi, S. Ferrandiz Bou, Radiative Darcy-Forchheimer Micropler Bödewadt flow of CNTs with viscous dissipation effect, *J. of Petroleum Science and Engineering* 217 (2022), 110857.
- [8] U. Farooq, H. Waqas, Z. Shah, P. Kumam, W. Deebani, On unsteady 3D bio-convection flow of viscoelastic nanofluid with radiative heat transfer inside a solar collector plate, *Sci. Rep.* 12 (2022) 2952.
- [9] T. Hayat, K. Muhammad, A. Alsaedi, Melting effect in MHD stagnation point flow of Jeffrey nanomaterial, *Phys. Scr.* 94 (2019), 115702.
- [10] G. Pavoski, F. Garjulli, C.R. dos Santos, M.L. Moraes, J.A.S. Tenório, D.C. R. Espinosa, Synthesis of a magnetic composite of silica with micro and nanocobalt metallic structures from a spent catalyst (Co<sub>3</sub>O<sub>4</sub>), *Mater. Sci. Eng., B* 285 (2022), 115921.
- [11] M.K. Nayak, MHD 3D flow and heat transfer analysis of nanofluid by shrinking surface inspired by thermal radiation and viscous dissipation, *Int J Mech Sci* 125 (2017) 185–193.
- [12] J. Chen, T. Nakate, Q.T. Nguyen, Y. Wei, S. Park, Surface activated Co<sub>3</sub>O<sub>4</sub>/MoO<sub>3</sub> nanostructured electrodes by air-plasma treatment toward enhanced super capacitor, *Mater. Sci. Eng., B* 285 (2022), 115928.
- [13] M.K. Nayak, A. Sattar Dogonchi, Y. Elmasry, N. Karimi, A.J. Chamkha, H. Alhumadeh, Free convection and second law scrutiny of NEPCM suspension inside a wavy-baffle-equipped cylinder under altered Fourier theory, *J. Taiwan Inst. Chem. Eng.* 128 (2021) 288–300.
- [14] T. Hayat, K. Muhammad, A. Alsaedi, B. Ahmed, Melting effect in squeezing flow of third-grade fluid with non-Fourier heat flux model, *Phys. Scr.* 94 (2019), 105705.
- [15] M.K. Nayak, F. Mabood, A.S. Dogonchi, W.A. Khan, Electromagnetic flow of SWCNT/MWCNT suspensions with optimized entropy generation and cubic auto catalysis chemical reaction, *Int. Commun. Heat Mass Transfer* 120 (2021), 104996.
- [16] A. Santos, L. Amorim, J.P. Nunes, A.F. Silva, J.C. Viana, Carbon nanotubes based multi-directional strain sensor, *Mater. Sci. Eng., B* 285 (2022), 115937.
- [17] S. Harish, G. Murugesan, J. Archana, M. Navaneetha, Amine-functionalized ZnO hierarchical nanostructures for enhanced photocatalytic decomposition under visible light illumination, *Mater. Sci. Eng., B* 285 (2022), 115844.
- [18] R. Mehmood, M.K. Nayak, N.S. Akbar, O.D. Makinde, Effects of thermal-diffusion and diffusion-thermo on oblique stagnation point flow of couple stress Casson fluid over a stretched horizontal Riga plate with higher order chemical reaction, *Journal of Nanofluids* 8 (1) (2019) 94–102.
- [19] F. Mabood, T. Muhammad, M.K. Nayak, H. Waqas, O.D. Makinde, EMHD flow of non-Newtonian nanofluids over thin needle with Robinson's condition and Arrhenius pre-exponential factor law, *Phys. Scr.* 95 (11) (2020), 115219.
- [20] M. Sajjad, F. Ahmad, L. Ali Shah, M. Khan, Designing graphene oxide/silver nanoparticles based nanocomposites by energy efficient green chemistry approach and their physicochemical characterization, *Mater. Sci. Eng., B* 284 (2022) 15899.
- [21] F.E. Alsaedi, K. Muhammad, T. Hayat, A. Alsaedi, S. Asghar, Numerical study of melting effect with entropy generation minimization in flow of carbon nanotubes, *J Thermal Analysis and Calorimetry* 140 (2020) 321–329.
- [22] J.R. Babu, K.K. Kumar, S.S. Rao, State-of-art review on hybrid nanofluids, *Renew. Sust. Energ. Rev.* 77 (2017) 551–565.
- [23] L. Yang, W. Ji, M. Mao, J.-N. Huang, An updated review on the properties, fabrication and application of hybrid-nanofluids along with their environmental effects, *J. Clean. Prod.* 257 (2020), 120408.
- [24] S. Suresh, K.P. Venkitaraj, P. Selvakumar, M. Chandrasekar, Effect of Al<sub>2</sub>O<sub>3</sub>-Cu/water hybrid nanofluid in heat transfer, *Exp. Thermal Fluid Sci.* 38 (2012) 54–60.
- [25] I. Waini, A. Ishak, I. Pop, Unsteady flow and heat transfer past a stretching/shrinking sheet in a hybrid nanofluid, *Int. J. Heat Mass Transf.* 136 (2019) 288–297.
- [26] M. Rooman, M. Asif Jan, Z. Shah, G. Alhawael, S. Iqbal, Entropy optimization in hybrid radiative nanofluid flow with effect of variable magnetic field over exponential stretching plate, *Waves in Random and Complex Media*, DOI: 10.1080/17455030.2022.2102268.
- [27] M.K. Nayak, N. Karimi, A.J. Chamkha, A. Sattar Dogonchi, S. El-Sapa, A.M. Galal, Efficacy of diverse structures of wavy baffles on heat transfer amplification of double-diffusive natural convection inside a C-shaped enclosure filled with hybrid nanofluid, *Sustainable Energy Technol. Assess.* 52 (2022), 102180.
- [28] K. Muhammad, T. Hayat, B. Ahmad, Joule heating in squeezed flow of hybrid nanomaterial via FDM with Cattaneo-Christov (C-C) heat flux, *Int. J. Num. Meth. Fluid Flow* 32 (8) (2022) 2573–2591.
- [29] M.K. Nayak, F. Mabood, A.S. Dogonchi, K.M. Ramadan, I. Tlili, Entropy optimized assisting and opposing non-linear radiative flow of hybrid nanofluid, *Waves Random Complex Medium* (2022), <https://doi.org/10.1080/17455030.2022.2032474>.
- [30] K. Muhammad, T. Hayat, S. Momani, S. Asghar, FDM analysis for squeezed flow of hybrid nanofluid in presence of Cattaneo-Christov (CC) heat flux and convective boundary condition, *Alexandria Engineering Journal* 61 (6) (2022) 4719–4727.
- [31] S. Shaw, S.S. Samantaray, A. Misra, M.K. Nayak, O.D. Makinde, Hydromagnetic flow and thermal interpretations of Cross hybrid nanofluid influenced by linear, nonlinear and quadratic thermal radiations for any Prandtl number, *Int. Commun. Heat Mass Transfer* 130 (2022), 105816.
- [32] W. Ahmed, S.N. Kazi, Z.Z. Chowdhury, M.R.B. Johan, S. Mehmood, E. M. Manzoore, M.A. Soudagar, M.G. Mujtaba, Muhammad Shakeel Ahmad, Heat transfer growth of sonochemically synthesized novel mixed metal oxide ZnO+ Al<sub>2</sub>O<sub>3</sub>+TiO<sub>2</sub>/DW based ternary hybrid nanofluids in a square flow conduit, *Renew. Sustain. Energy Rev.* 145 (2021), 111025.
- [33] A. Dezfulizadeh, A. Aghaei, A.H. Joshaghani, M.M. Najafzadeh, An experimental study on dynamic viscosity and thermal conductivity of water-Cu-SiO<sub>2</sub>-MWCNT ternary hybrid nanofluid and the development of practical correlations, *Powder Technol.* 389 (2021) 215–234.
- [34] R.R. Sahoo, V. Kumar, Development of a new correlation to determine the viscosity of ternary hybrid nanofluid, *Int. Commun. Heat Mass Transfer* 111 (2020), 104451.
- [35] M.K. Sarangi, D.N. Thatoi, M.K. Nayak, J. Prakash, K. Ramesh, M. Azam, Rotational flow and thermal behavior of ternary hybrid nanomaterials at small and high Prandtl numbers, *Int. Commun. Heat Mass Transfer* 138 (2022), 106337.
- [36] V.U. Bödewadt, Die drehströmungüberfestemgrunde. *ZAMM-Journal of Applied Mathematics and Mechanics/ZeitschriftfürAngewandteMathematik und, Mechanik* 20 (5) (1940) 241–253.
- [37] M. Turkyilmazoglu, Bödewadt flow and heat transfer over a stretching stationary disk, *Int. J. Mech. Sci.* 90 (2015) 246–250.
- [38] T. Rafiq, M. Mustafa, Bödewadt flow of Bingham fluids over a non-isothermal permeable disk with viscous dissipation effects, *Alexandria Engineering Journal* 60 (3) (2021) 2857–2864.
- [39] D. Mukherjee, B. Sahoo, The effects of Coriolis force and radial stretch on the convective instability characteristics of the Bödewadt flow, *Proceedings of the Institution of Mechanical Engineers, Part C: Journal of Mechanical Engineering Science* 235 (22) (2021) 6170–6176.
- [40] Y. Do, J.M. Lopez, F. Marques, Optimal harmonic response in a confined Bödewadt boundary layer flow, *Phys. Rev. E* 82 (3) (2010), 036301.
- [41] B. Sahoo, S. Abbasbandy, S. Poncet, A brief note on the computation of the Bödewadt flow with Navier slip boundary conditions, *Comput. Fluids* 90 (2014) 133–137.
- [42] T. Von Kármán, Über laminare und turbulente reibung, *Z. Angew. Math. Mech.* 1 (1921) 233–252.
- [43] M. Mustafa, J.A. Khan, T. Hayat, A. Alsaedi, On Bödewadt flow and heat transfer of nanofluids over a stretching stationary disk, *J. Mol. Liq.* 211 (2015) 119–125.
- [44] P. Sibanda, O.D. Makinde, On steady MHD flow and heat transfer past a rotating disk in a porous medium with Ohmic heating and viscous dissipation, *Int. J. Num. Meth. Fluid Flow* 20 (3) (2010) 269–285.
- [45] K. Muhammad, T. Hayat, A. Alsaedi, B. Ahmad, Numerical study of entropy production minimization in Bödewadt flow with carbon nanotubes, *Physica A* 550 (2020), 123966.
- [46] S.Z. Abbas, M. Ijaz Khan, S. Kadry, W.A. Khan, M. Israr-Ur-Rehman, M. Waqas, Fully developed entropy optimized second order velocity slip MHD nanofluid flow with activation energy, *Comput. Methods Programs Biomed.* 190 (2020), 105362.
- [47] S. Kashyap, J. Sarkar, A. Kumar, Performance enhancement of regenerative evaporative cooler by surface alterations and using ternary hybrid nanofluids, *Energy* 225 (2021), 120199.
- [48] R.R. Sahoo, Thermo-hydraulic characteristics of radiator with various shape nanoparticle-based ternary hybrid nanofluid, *Powder Technol.* 370 (2020) 19–28.
- [49] Z. Shah, M.R. Hajizadeh, N.A. Ikramullah, W. Alreshidi, M.S. Deebani, Entropy optimization and heat transfer modeling for Lorentz forces effect on solidification of NEPCM, *Int. Commun. Heat Mass Transfer* 117 (2020), 104715.
- [50] M. Shutaywi, M. Rooman, M.A. Jan, N. Vrinceanu, Z. Shah, W. Deebani, Entropy Generation and Thermal Analysis on MHD Second-Grade Fluid with Variable thermophysical Properties over a Stratified Permeable Surface of Paraboloid Revolution, *ACS Omega* 7 (2022) 27436–27449.
- [51] M. Rooman, M.A. Jan, Z. Shah, N. Vrinceanu, S.F. Bou, S. Iqbal, W. Deebani, Entropy Optimization on Axisymmetric Darcy-Forchheimer Powell-Eyring Nanofluid over a Horizontally Stretching Cylinder with Viscous Dissipation Effect, *Coatings* 12 (6) (2022) 749.
- [52] Z. Shah, M. Jafaryar, M. Sheikholeslami, Ikramullah, P. Kumam, Heat transfer intensification of nanomaterial with involve of swirl flow device concerning entropy generation, *Scient. Rep.*, 11 (2021) 12.